Corner modes in Non-Hermitian long-range model

Arnob Kumar Ghosh,[1,2,3] Arijit Saha,[1,2,*] and Tanay Nag[4,†]

[1] Institute of Physics, Sachivalaya Marg, Bhubaneswar-751005, India
[2] Homi Bhabha National Institute, Training School Complex, Anushakti Nagar, Mumbai 400094, India
[3] Department of Physics and Astronomy, Uppsala University, Box 516, 75120 Uppsala, Sweden
[4] Department of Physics, BITS Pilani-Hyderabad Campus, Telangana 500078, India

We consider non-Hermitian (NH) analog of a second-order topological insulator, protected by chiral symmetry, in the presence of second-nearest neighbor hopping elements to theoretically investigate the interplay between long-range and topological order away from Hermiticity. In addition to the four zero-energy corner modes present in the first nearest neighbor hopping model, we uncover that the second nearest neighbor hopping introduces another topological phase with sixteen zero-energy corner modes. Importantly, the NH effects are manifested in altering the Hermitian phase boundaries for both the models. While comparing the complex energy spectrum under open boundary conditions, and bi-orthogonalized quadrupolar winding number (QWN) in real space, we resolve the apparent anomaly in the bulk boundary correspondence of the NH system as compared to the Hermitian counterpart by incorporating the effect of non-Bloch form of momentum into the mass term. The above invariant is also capable of capturing the phase boundaries between the two different topological phases where the degeneracy of the corner modes is evident, as exclusively observed for the second nearest neighbor model.

arXiv:2403.19765v1 [cond-mat.mes-hall] 28 Mar 2024

I. INTRODUCTION

The systems with topological band properties are identified with gapless boundary modes that are characterized by symmetry-protected topological invariants. This is known as bulk boundary correspondence (BBC) [1, 2]. The conventional BBC, being an integral part of the first-order ($n = 1$) topological phase [1, 3–5], is generalized for higher-order ($n > 1$) topological phases in $d \geq 2$ dimensions where there exist $n_c = (d - n)$-dimensional boundary modes [6–40]. For example, the second-order topological insulator (SOTI) hosts zero-dimensional (0D) localized corner modes at zero-energy while this phase is characterized by nested polarization or quadrupolar moment. Very recently, it has been reported that the number of boundary modes in a topological phase can be tuned by considering long-range hopping terms [41–44] as well as by implementing periodic Floquet drive [39, 45]. Once the extended model continues to preserve the chiral symmetry (CS), one can characterize the new topological phase by winding numbers in odd spatial dimension [46–48]. The number of degenerate zero-energy states at each boundary increases according to the enhancement of the range of the hopping amplitudes as indicated by the winding number ensuring the BBC [49, 50]. It is noteworthy that one-dimensional winding number for the first-order topological systems becomes passive in case of even-dimensional generalizations [51]. In contrast, the higher-order topological (HOT) phase in even spatial dimension can be characterized by an appropriately defined winding number preserving CS as a constraint [52].

In recent years, thanks to the practical realization of higher-order topological phases in meta-materials [53–56] where energy conservation no longer holds [57, 58] and the domain of topological quantum matter can be extended to the non-Hermitian (NH) systems. The coupling to the environment [59–61], disorder/interaction-mediated quasiparticles with finite lifetime [62–64] can effectively induce a complex self energy that is modeled by an NH effective Hamiltonian [58, 65–71]. Interestingly, the non-Bloch nature of the wavefunction for the NH systems renormalizes the topological mass term, thus enriching the BBC such that topological phase transitions perceived with open-boundary conditions can be explained by an appropriate bulk invariant [72–79]. The NH topological systems showcase various intriguing features such as the skin effect where the bulk states accumulate at the boundary [72, 73, 75, 80], exceptional points where eigenstates, corresponding to the degenerate bands, coalesce [81, 82].

Going beyond the scope of short-range hopping, long-range hopping in Hermitian systems is found to mediate versatile topological phases where the number of zero-energy modes increases [44, 83–85]. In this context, the interplay between long-range hopping elements and non-Hermiticity is still in its infancy as far as HOT systems are concerned [74, 86–89]. Therefore, considering a two-dimensional (2D) long-range NH SOTI, we, therefore, examine whether non-Hermiticity induces exceptional SOTI phases, otherwise absent in the Hermitian case, and address the following interesting questions that have not been explored so far in literature, to the best of our knowledge: How does the BBC change in the above NH phases? Can we characterize these emerging exceptional topological phases by bi-orthogonalized non-Bloch winding number?

We consider a CS-preserved generic model, hosting SOTI phases in the presence of non-Hermiticity and long-range hopping terms. The first [second] nearest neighbor (NN) Hermitian model Hamiltonian can host four

* arijit@iopb.res.in
† tanay.nag@hyderabad.bits-pilani.ac.in

[four and sixteen] zero-energy corner modes while exceptional points, caused by the NH effects, reshape topological phase boundaries as compared to the Hermitian case. As a result, we find that BBC is not only different from their Hermitian counterparts but also non-trivially modified once long-range terms are included. The phase boundaries between four [one] and one [none] zero-energy modes per corner in the second [first] NN model are revised following the dressed mass term due to the non-Bloch nature of wavefunction for NH Hamiltonian. We compute the quadrupolar winding number (QWN) appropriately in real space by exploiting the CS as well as implementing the bi-orthogonalization and non-Bloch nature to lay out the phase diagram which is in accordance with the complex spectrum under open boundary conditions (OBC).

The remainder of the article is organized in the following way. We discuss the details of the tight-binding Hamiltonian in Sec. II, where both the NH short-range and relatively long-range models are demonstrated. Sec. III is devoted to the main results of this article. In particular, we discuss the result associated with the first and the second NN neighbor hopping models in Secs. III A and III B, respectively. Next, we illustrate the exceptional phase diagram in Sec. III C by examining the QWN. We finally summarize and conclude in Sec. IV.

II. MODEL HAMILTONIAN

We consider the SOTI model in the presence of the second NN hopping as follows [86]

$$H_0(\mathbf{k}) = (\lambda_1^s \sin k_x + \lambda_2^s \sin 2k_x)\,\Gamma_1 + (\lambda_1^s \sin k_y + \lambda_2^s \sin 2k_y)\,\Gamma_2 + \left[m_0 - \lambda_1^h (\cos k_x + \cos k_y) - \lambda_2^h (\cos 2k_x + \cos 2k_y)\right]\Gamma_3 + \left[\lambda_1^f (\cos k_x - \cos k_y) + \lambda_2^f (\cos 2k_x - \cos 2k_y)\right]\Gamma_4 \;, \tag{1}$$

where, $\Gamma_1 = \sigma_x s_z$, $\Gamma_2 = \sigma_y s_0$, $\Gamma_3 = \sigma_z s_0$, $\Gamma_4 = \sigma_x s_x$. We consider strengths of first (second) NN hopping, spin-orbit coupling, and C_4 symmetry breaking mass terms as λ_1^h, λ_1^s, and λ_1^f, (λ_2^h, λ_2^s, and λ_2^f) respectively. Here, m_0 is the staggered mass term. In what follows, we refer to the case of $\lambda_1 \neq 0$ and $\lambda_2 = 0$ ($\lambda_{1,2} \neq 0$) as first (second) NN model. The SOTI phase with four zero-energy corner modes arises for $-2\lambda_1^h < m_0 < 2\lambda_1^h$ when ($\lambda_1^f, \lambda_2^f = 0$). The SOTI phases with four and sixteen zero-energy corner modes exist for $-2\lambda_2^h < m_0 < 0$ and $0 < m_0 < 2\lambda_1^h + 2\lambda_2^h$, respectively when $\lambda_{1,2}^f \neq 0$. Note that, this model also hosts first order topological insulator phase for $-2\lambda_1^h < m_0 < 2\lambda_1^h$ and $-2\lambda_2^h < m_0 < 2\lambda_1^h + 2\lambda_2^h$, respectively, when $(\lambda_1^f, \lambda_2^f) = (\neq 0, 0)$ and $(\neq 0, \neq 0)$. Interestingly, there is a topological phase transition that occurs at $m_0 = 0$ for the second NN model only. The above model preserves particle-hole symmetry (PHS) $P = A\mathcal{K}$ and CS $C = \sigma_x s_y$ such that $PH_0(\mathbf{k})P^{-1} = -H_0(-\mathbf{k})$ and $CH_0(\mathbf{k})C^{-1} = -H_0(\mathbf{k})$ with $A = \sigma_x s_z$ and $\mathcal{K}$ being the complex-conjugation. Importantly, the time-reversal symmetry $T = B\mathcal{K}$ is broken when $\lambda_{1,2}^f \neq 0$ such that $TH_0(\mathbf{k})T^{-1} \neq H_0(-\mathbf{k})$ with $B = \sigma_0 s_y$.

Having demonstrated the physics of Hermitian SOTI model, we now focus on the NH version of the above. We associate the NH effect to the spin-orbit coupling part of the above Hamiltonian: $H_\gamma(\mathbf{k}) = H_0(\mathbf{k}) + i\gamma(\Gamma_1 + \Gamma_2)$ resulting in $H_\gamma^\dagger(\mathbf{k}) \neq H_\gamma(\mathbf{k})$. The non-Hermiticity considered here can be thought of as an imaginary fictitious Zeeman field [67, 86]. Notice that $H_\gamma(\mathbf{k})$ preserves PHS, generated by A as follows $AH_\gamma^*(\mathbf{k})A^{-1} = -H_\gamma(-\mathbf{k})$. The CS continues to be preserved as $CH_\gamma(\mathbf{k})C^{-1} = -H_\gamma(\mathbf{k})$. We exploit the CS to define the NH analog of quadrupole moment in real space (see latter text for discussion). In the rest of the paper, we consider $\lambda_{1,2}^h = 1$ for the sake of simplicity.

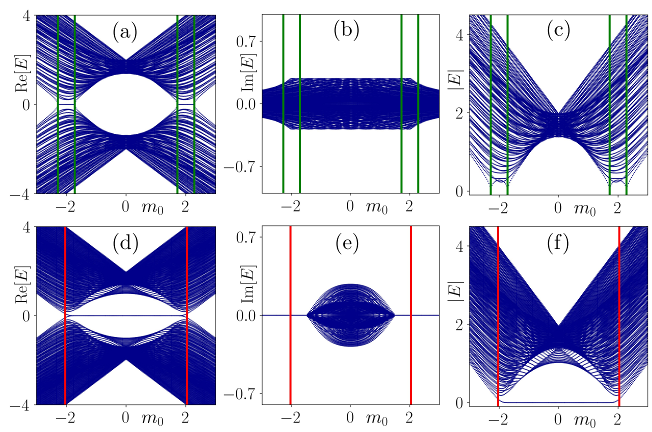

FIG. 1. The energy spectra under PBC and OBC are illustrated as function of the staggered mass term m_0 in upper and lower panels, respectively, for first NN hopping. The above panels correspond to (a,d) Re[E], (b,e) Im[E] and (c,f) $|E|$. The model parameters are chosen as $\lambda_1^s = \lambda_1^h = \lambda_1^f = 1.0$, and $\gamma = 0.2$. Here, green lines correspond to the exceptional points obtained from the PBC case $m_0 = \pm 2 \pm \tilde{\gamma}$. The red lines, representing the exceptional phase boundary under OBC, are given by $m_0 = \pm(2 + \gamma_1^2)$.

III. RESULTS

In this section, we discuss the main results of this manuscript. We analyze the eigenvalue spectra and local density of states (LDOS) corresponding to our NH

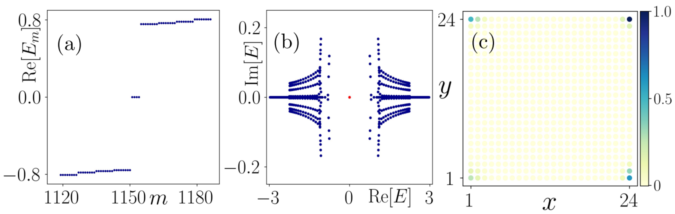

FIG. 2. (a) The real part of the energy eigenvalue spectrum $\mathrm{Re}[E_m]$ obtained under OBC is shown as a function of the state index m. (b) The eigenvalue spectrum in the $\mathrm{Re}[E]$-$\mathrm{Im}[E]$ plane is illustrated. The eigenvalues corresponding to the corner state are marked by the red dots. (c) The LDOS spectra associated with the $\mathrm{Re}[E] = 0$ is depicted in the 2D domain. We choose $m_0 = 1.0$, while the other model parameters remain the same as mentioned in Fig. 1.

model with first and second NN hopping. Afterward, we define the quadrupolar winding number for our system and demonstrate the phase diagram.

A. NH Model with first NN hopping

We begin with the energy dispersion of the NH SOTI model in the presence of the first NN, as shown in Figs. 1 (a,b,c) [(d,e,f)] under periodic boundary condition (PBC) [(OBC)]. While employing PBC, we find $\mathrm{Re}[E] = 0$ for $2 - \tilde{\gamma} < m_0 < 2 + \tilde{\gamma}$ and $-2 - \tilde{\gamma} < m_0 < -2 + \tilde{\gamma}$ with $\tilde{\gamma} = \sqrt{2\gamma^2}$ around $m_0 = \mp 2$ as depicted by the gapless regions in Fig. 1(a), bounded by the green lines. These exceptional boundaries around $m_0 = 2, -2$, respectively, can be understood from the two-fold degeneracies of energy bands at $\mathbf{k} = (0, 0)$ and (π, π) such that $|E(\mathbf{k}_{\mathrm{EP}})| = 0$. Interestingly, these bulk gapless exceptional points $m_0 = \pm 2 \pm \tilde{\gamma}$ are exclusively noticed in $|E|$ under the PBC case as depicted in Fig. 1(c) by the green lines.

We find that the complex energy spectra obtained under OBC and depicted in Figs. 1(d,e,f) do not mimic the underlying PBC nature. One can observe SOTI modes for which the real part of energy vanishes according to $-2 - \gamma_1^2 < m_0 < 2 + \gamma_1^2$ with $\gamma_1 = \gamma/\lambda_1^s$ as depicted by the red lines in Fig. 1(d). These boundaries can be anticipated by the non-Bloch form of momentum $k_i \to k_i' - i\gamma/\lambda_1^s$ with $i = x, y$ where the renormalized mass term $m_0' = m_0 - 2 - \gamma_1^2 < 0$ (> 0) determines the topological (trivial) phase of the NH model [67, 86]. Note that, for Bloch momentum $\mathbf{k} = (0, 0)$ [$\mathbf{k} = (\pi, \pi)$], the exceptional phase boundaries extend till $m_0 = \pm(2 + \gamma_1^2)$ leading to the emergence of exceptional SOTI phases beyond the Hermitian gapless phase boundaries $m_0 = \pm 2$. All the single-particle energy states under OBC except the corner modes exhibit an imaginary component of energy for $|m_0| < 2$ as shown in Fig. 1(e). This is markedly different from the PBC case, depicted in Fig. 1(b), where single particle states have finite amount of imaginary energy for $|m_0| > 2$. This refers to a macroscopic degeneracy within a certain range of m_0 as far as the $\mathrm{Im}[E]$ is considered. Since such macroscopic degeneracy does not exist for $\mathrm{Re}[E]$, the $|E|$ demonstrates the NH corner modes for $|m_0| < |2 + \gamma_1^2|$ under OBC [see red lines in Fig. 1(f)], while non-Hermiticity mediated bulk gapless points are noticed for the PBC case, see Fig. 1(c).

Having understood the generation of the NH SOTI phase as a function of the topological mass m_0, we consider a slice with $m_0 = 1$ from Fig. 1 and analyze the results presented in Fig. 2. In particular, employing OBC, we depict the real part of the eigenvalue spectrum $\mathrm{Re}[E_m]$ close to $\mathrm{Re}[E] = 0$ as a function of the state index m in Fig. 2(a).We observe the appearence of four states at $\mathrm{Re}[E] = 0$, which corresponds to localized corner states. In Fig. 2(b), we illustrate the eigenvalue spectrum in the $\mathrm{Re}[E]$-$\mathrm{Im}[E]$ plane. The corner modes are marked by the red dot, which indicates that the corner modes have both real and imaginary parts of the eigenvalue equal to zero. The CS of the model is reflected in the symmetric profile of energy in positive and negative sides of the real energy, while the line gap nature is clearly observed. Moreover, we show the site-resolved LDOS distribution in Fig. 2(c). We find that the corner modes are mostly localized at only one corner of the 2D domain. This phenomenon of the localization of the corner modes limited to only one corner of the system has been investigated previously in an NH higher-order systems where mirror symmetries play a crucial role [74, 86].

B. NH Model with second NN hopping

To start with, we depict the energy dispersion of the NH SOTI model in the presence of the second NN in Figs. 3 (a,b,c) [(d,e,f)] under PBC [OBC]. We find degenerate eigenstate with $\mathrm{Re}[E] = 0$ under PBC for $-2 - \tilde{\gamma} < m_0 < -2 + \tilde{\gamma}$, $-\tilde{\gamma} < m_0 < \tilde{\gamma}$, and $4 - \tilde{\gamma} < m_0 < 4 + \tilde{\gamma}$ as depicted by the green lines in Fig. 3(a). These exceptional boundaries around $m_0 = -2$, 0 and 4, respectively, can be understood from the two-fold degeneracies of energy bands at $\mathbf{k} = (\pm 2\pi/3, \pm 2\pi/3)$, (π, π), and $(0, 0)$ such that $|E(\mathbf{k}_{\mathrm{EP}})| = 0$. Similar to the earlier first NN model, these bulk gapless exceptional points $m_0 = -2 \pm \tilde{\gamma}$, $\pm\tilde{\gamma}$, and $4 \pm \tilde{\gamma}$ are exclusively observed in $|E|$ for PBC case as depicted in Fig. 3(c) by green lines.

We now examine the energy spectrum for the second NN model in Figs. 3(d,e,f) employing OBC. Similar to the first NN case, the momentum takes the following non-Bloch form $k_i \to k_i' - i\gamma_2$ with $\gamma_2 = \gamma/(\lambda_1^s + 2\lambda_2^s)$ and $i = x, y$. This leads to the renormalized mass term $m_0' = m_0 - 4 - 5\gamma_2^2 < 0$ (> 0) for the topological (trivial) phase with zero-energy (finite energy bulk) modes considering the Bloch momentum $\mathbf{k} = (0, 0)$. On the other hand, another topological (trivial) phase with zero-energy (finite energy) modes appears for $-m_0' = m_0 + 2 + \gamma_2^2 > 0$ (< 0) while exploiting energy around the Bloch momentum $\mathbf{k} = (\pm 2\pi/3, \pm 2\pi/3)$. Our analy-

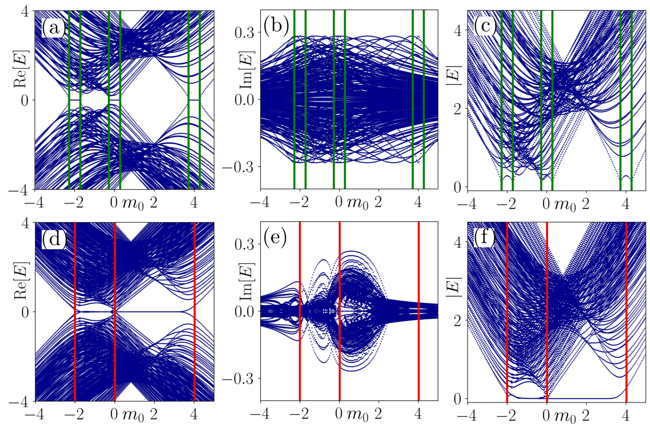

FIG. 3. The energy spectra under PBC and OBC are illustrated in upper and lower panels, respectively as a function of m_0, for second NN hopping. The panels correspond to (a,d) Re[E] (b,e) Im[E] and (c,f) $|E|$. We choose the model parameters as $\lambda_1^s = \lambda_1^h = \lambda_1^f = 1.0$, $\lambda_2^s = \lambda_2^h = \lambda_2^f = 1.0$ and $\gamma = 0.2$. The green lines correspond to the exceptional points $m_0 = 4 \pm \tilde{\gamma}$, $\pm\tilde{\gamma}$, and $-2 \pm \tilde{\gamma}$ under PBC. The red lines, representing the exceptional phase boundary under OBC, are given by $m_0 = 4 + 5\gamma_2^2$, $3\gamma_2^2$, and $-2 - \gamma_2^2$.

sis indicates the existence of four [sixteen] corner modes for $3\gamma_2^2 < m_0 < 4 + 5\gamma_2^2$ [$-2 - \gamma_2^2 < m_0 < 3\gamma_2^2$] yielding Re[$E$] = 0 under OBC. However, the numerical findings shown in Fig. 3(d) and the topological regime highlighted by the red lines, do not fully match with the exceptional boundaries predicted analytically. This can be attributed to the finite size effect in the second NN case, which is substantially small for the first NN case. We find macroscopic degeneracies at Re[E] = 0 around $m_0 = 0$, unlike the previous case. The complex energy spectrum Im[E] does not manifest any noteworthy features, as shown in Figs. 3(b,e), irrespective of PBC and OBC cases. The absolute value of energy is expected to vanish i.e., $|E| = 0$ under OBC for $-2 - \gamma_2^2 < m_0 < 4 + 5\gamma_2^2$. However, numerical results suffer from finite size effects as far as the exceptional boundaries are concerned [see the red lines in Fig. 3(f)]. The finite value of γ (NH effect) thus extends the Hermitian topological phase beyond its boundaries, leading to exceptional topological phases.

Moreover, we also analyze the eigenvalue spectrum choosing a fixed value of m_0. As discussed before, we obtain four corner states when $3\gamma_2^2 < m_0 < 4 + 5\gamma_2^2$. The corresponding eigenvalue spectrum and LDOS, when the system exhibits four corner states, remain qualitatively the same as depicted in Fig. 2 for the first NN case. Thus, we do not repeat that analysis here. Rather, we choose the value of m_0 in such a way that we obtain sixteen corner states. For this case, we show the real part of the eigenvalue spectrum Re[E_m] close to Re[E] = 0 as a function of the state index m in Fig. 4(a), for a system obeying OBC. One can note the existence of sixteen states at Re[E] = 0, which corresponds to localized corner modes. The finite separation from the exact Re[E] = 0 can be attributed to the finite size effect. Nevertheless, in Fig. 4(b), we illustrate the eigenvalue spectrum in the Re[E]-Im[E] plane where the CS manifests itself in the symmetric profile of real energy. The corner modes are marked by the red dot. The line gap feature behaves in the similar way like the previous case. The corner modes have both real and imaginary parts of the eigenvalue equal to zero. We also illustrate the site-resolved LDOS distribution in Fig. 4(c). We find that the corner modes are mostly localized at only one corner of the 2D system, similar to the first NN hopping case.

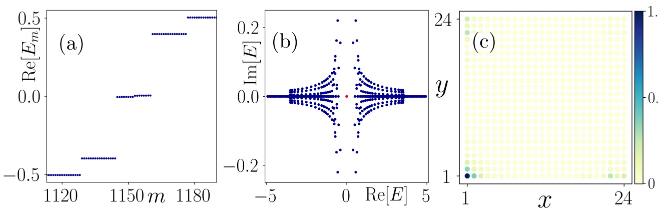

FIG. 4. (a) The real part of the energy spectrum Re[E_m] obtained under OBC is shown as a function of the state index m. (b) The eigenvalue spectrum in the Re[E]-Im[E] plane is demonstrated. The corner state eigenvalues are indicated by the red dot. (c) The LDOS associated with the Re[E] = 0 is depicted in the 2D lattice. We choose $m_0 = -1.0$, while the other model parameters remain the same as mentioned in Fig. 3.

C. Quadrupole Winding number

We now investigate the topological invariant, namely, quadrupole winding number (QWN), by exploiting the CS. In the following discussion, we first illustrate the Hermitian version of QWN. Given the fact that CS constraints $CH_0(\mathbf{k})C^{-1} = -H_0(\mathbf{k})$, we can anti-diagonalize the Hamiltonian in the basis of the CS operator spanned by U_C as follows [48, 90]

$$\tilde{H}_0 = U_C^\dagger H_0 U_C = \begin{pmatrix} 0 & h \\ \tilde{h} & 0 \end{pmatrix} , \tag{2}$$

Here, $\tilde{h} = h^\dagger$ if $\tilde{H}_0$ is Hermitian. We find $U_C C U_C^\dagger = \pm 1$, suggesting that CS can be classified into two kinds of sublattices, namely A and B for $+$ and $-$ expectation values, respectively. This further entails that $U_C = U_C^A - U_C^B$ where $U_C^A = \sum_{\alpha\in A} |\alpha\rangle\langle\alpha|$ and $U_C^B = \sum_{\beta\in B} |\beta\rangle\langle\beta|$.

Employing singular value decomposition of h, we obtain $h = U_A \Sigma U_B^\dagger$ where $U_{A,B}$ are unitary matrices and Σ denotes a diagonal matrix. Note that, the diagonal elements of Σ are referred to as singular values. One can compute the flattened Hamiltonian Q, having eigenvalue ± 1 as follows [52]

$$Q = \begin{pmatrix} 0 & q \\ q^\dagger & 0 \end{pmatrix} , \tag{3}$$

with $q = U_A U_B^\dagger$ being a unitary matrix. It has been shown that the winding number, derived using q and $q^\dagger$, is related to the relative polarization of A and B sublattice. In a similar spirit, the winding number in the real space is given by [91]

$$\nu = \frac{1}{2\pi i}\mathrm{Tr}\left[\log\left(\mathcal{X}_A \mathcal{X}_B^\dagger\right)\right] \ , \tag{4}$$

where, $\mathcal{X}_\sigma = U_\sigma^\dagger U_C^\sigma \mathcal{X} U_C^\sigma U_\sigma$ ($\sigma = A, B$) are unitary matrices. The operator $\mathcal{X}_\sigma$ denotes the sublattice dipole operator, which is the projection of the position operator onto the σ sector of the chiral basis. The position operator, i.e., the dipole operator $\mathcal{X} = \exp(2i\pi x/L)$ is defined on a periodic array of one-dimensional length L.

Now turning to the two-dimensional system where the dipole operator $\mathcal{X}$ can be replaced by the quadrupole operator $\mathcal{Q} = \exp(2i\pi xy/L_x L_y)$. This results in the sublattice quadrupole operator $\mathcal{Q}_\sigma = U_\sigma^\dagger U_C^\sigma \mathcal{Q} U_C^\sigma U_\sigma$. Therefore, the QWN can be defined as [52]

$$N_{xy} = \frac{1}{2\pi i}\mathrm{Tr}\left[\log\left(\mathcal{Q}_A \mathcal{Q}_B^\dagger\right)\right] \ , \tag{5}$$

This invariant is quantized to an integer number and predicts the number of topologically protected corner states at each corner of the 2D lattice.

We now examine the present situation with $\gamma \neq 0$ where the NH analog of QWN is discussed. Importantly, CS is also preserved for the NH Hamiltonian $CH_\gamma(\mathbf{k})C^{-1} = -H_\gamma(\mathbf{k})$ allowing for the anti-diagonal form of $\tilde{H}_\gamma$. At the same time, the definition of $U_C^{A,B}$ remains unaltered for the NH case. We adopt the bi-orthogonalized definitions of U_A and $U_B^\dagger$, obtained from the singular value decomposition of h, to define $U_A^\dagger$ and U_B, respectively. One has to ensure $\sum_n |U_{\sigma,n}^R\rangle\langle U_{\sigma,n}^L| = \mathbb{1}$ and $\langle U_{\sigma,n}^L | U_{\sigma,m}^R\rangle = \delta_{mn}$ with $\sigma = A, B$ and $L(R)$ denotes the left (right) eigenvectors. This results in left [right] eigenvector corresponding to right eigenvector $(U_B^\dagger)^\dagger \equiv U_B^R$ [left eigenvector $U_A^\dagger \equiv U_A^L$] as $U_B^\dagger \equiv U_B^L$ [$U_A \equiv U_A^R$]. Therefore, sublattice quadrupole operator $\mathcal{Q}_\sigma$ takes the form $\mathcal{Q}_\sigma = U_\sigma^L U_C^\sigma \mathcal{Q} U_C^\sigma U_\sigma^R$. In addition, the non-Bloch form of momentum has to be incorporated while computing $\mathcal{Q}_\sigma$.

To be precise, the complex momentum $k_i \to k_i' - i\gamma_2$ with $i = x, y$ leads to the exponentially enhanced and suppressed hopping elements by the multiplicative factors $\exp(\gamma_1)$ and $\exp(-\gamma_1)$ [$\exp(\gamma_2)$ and $\exp(-\gamma_2)$] for first [second] NN models. We use the real space form of the tight-binding model with the renormalized hopping amplitudes as follows $\lambda_{1,2}^{s,h,f} \to \lambda_{1,2}^{s,h,f}\exp(\gamma_{1,2})$ and $\lambda_{1,2}^{s,h,f} \to \lambda_{1,2}^{s,h,f}\exp(-\gamma_{1,2})$ for forward and backward hopping amplitudes, respectively. We consider the real space version of NH Hamiltonian H_γ with the above mentioned renormalized hoppings in order to compute QWN. Altogether this enables us to define the NH analog of QWN N_{xy} with dressed hopping and bi-orthogonalized definition. Note that, the real part of N_{xy} exhibits quantized value for the present case with $\gamma \neq 0$ as demonstrated below.

We now discuss the phase diagram of the first and second NN NH model in the γ-m_0 plane in Figs. 5(a,b) respectively. Note that, there exists four corner modes with $\mathrm{Re}[E] = 0$ for $m_0 < 2 + \gamma_1^2$, yielding $N_{xy} = 1$. This refers to the fact that there exists only one topological zero-mode per corner [see Fig. 5(a)]. On the other hand, when $m_0 > 2 + \gamma_1^2$, the NH model does not host any topological phase and hence $N_{xy} = 0$. Hence, the topological phase boundary is $m_0 = 2 + \gamma_1^2$ which is indicated by the yellow solid line. This is also predicted from the complex energy spectrum with OBC. The yellow dashed lines in Fig. 5(a) represent $m_0 = 2 \pm \tilde{\gamma}$ lines as predicted from the complex energy under PBC. Interestingly, the real space invariant QWN fails to identify these phase boundaries. Unlike the Hermitian system, the phase boundaries between topological and trivial phases cannot be captured by the energy spectrum under OBC and PBC in the present NH case. This clearly suggests that the topological phase, predicted from the complex energy spectrum in OBC, is apprehended by the non-Bloch and bi-orthogonalized version of QWN. We note that the analytically derived phase boundaries are valid for $\gamma_{1,2} \ll 1$.

We find qualitatively similar results in case of the second NN model as shown in Fig. 5(b). In addition to $N_{xy} = 1$ phase, we obtain $N_{xy} = 4$ phase where four zero-energy modes with $\mathrm{Re}[E] = 0$ are present at each corner. While investigating the phase boundaries, it is expected to find $N_{xy} = 1$ [4] for $3\gamma_2^2 < m_0 < 4 + 5\gamma_2^2$ [$-2 - \gamma_2^2 < m_0 < 3\gamma_2^2$]. For smaller strength of non-Hermiticity i.e., $\gamma \to 0$, we find quantitative agreement between the analytical and numerical findings. The phase boundaries $m_0 = 4 + 5\gamma_2^2$, $3\gamma_2^2$, and $-2 - \gamma_2^2$, designated by the yellow solid line, do not fully comply with the N_{xy} profile for $\gamma > 0.1$. This can be due to more intricacies than just the finite size effect. Interestingly, the following tendency is noticed: for $\tilde{\gamma} < m_0 < 4 + 5\gamma_2^2$, one obtains $N_{xy} = 1$ while within the regime $-2 - \tilde{\gamma} < m_0 < -\tilde{\gamma}$, N_{xy} acquires the value 4. Therefore, the non-Bloch and bi-orthogonalized version of QWN can quantitatively and qualitatively identify the phase boundaries of SOTI phases hosting four and sixteen corner modes starting from the trivial phases for $m_0 > 4 + 5\gamma_2^2$ and $m_0 < -2 - \tilde{\gamma}$, respectively, across which N_{xy} jumps between zero and finite values. The real space invariant QWN is thus a useful topological marker to identify the exceptional phases for our NH system with OBC.

On the other hand, between two SOTI phases with different number of corner modes (for $-\tilde{\gamma} < m_0 < \tilde{\gamma}$), we find $N_{xy} \neq 0$ as depicted in Fig. 5(b). In the complex energy analysis under OBC, we find macroscopic degeneracies with $\mathrm{Re}[E] = 0$ for $-2 - \gamma_2^2 < m_0 < \tilde{\gamma}$. Likewise the earlier first NN case, N_{xy} does not exhibit any jumps between finite and zero values around $m_0 = 4 \pm \tilde{\gamma}$ and $m_0 = -2 \pm \tilde{\gamma}$ which are predicted by the complex energy spectrum under PBC. On the contrary, $m_0 = \pm\tilde{\gamma}$ boundaries, predicted by complex energy spectrum un-

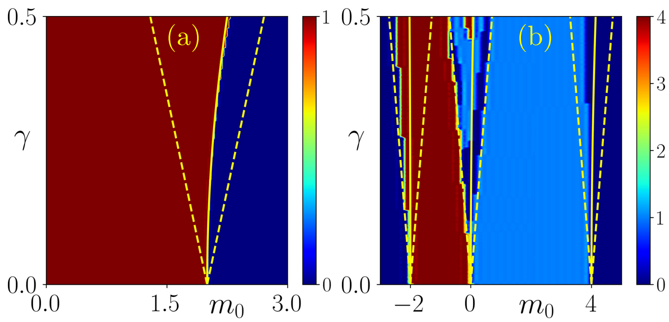

FIG. 5. The phase diagram in m_0-γ plane for NH first NN and second NN hopping models are shown in panel (a), and (b), respectively. The color bar represents QWN N_{xy}. The phase boundary $m_0 = 2+\gamma_1^2$ [$m_0 = 2\pm\tilde{\gamma}$], obtained from OBC [PBC], between exceptional topological and trivial phases in panel (a) is identified by the yellow solid [dashed] line. The phase boundaries, associated with OBC [PBC], between topological phases hosting sixteen and four corner modes, and trivial phase are given by $m_0 = 4 + 5\gamma_2^2$ [$m_0 = 4 \pm \tilde{\gamma}$], $m_0 = 3\gamma_2^2$ [$m_0 = \pm\tilde{\gamma}$], and $m_0 = -2 - \gamma_2^2$ [$m_0 = -2 \pm \tilde{\gamma}$], respectively, represented by the yellow solid [dashed] lines in panel (b).

der PBC, are visible as N_{xy} changes between two finite values. The exceptional lines $m_0 = -2 \pm \tilde{\gamma}$, $\pm\tilde{\gamma}$, and $4 \pm \tilde{\gamma}$ obtained employing PBC are depicted by yellow dashed lines in Fig. 5(b). This agreement is surprising and yet to be explored in the future. However, there is an apparent discrepancy between the solid yellow lines and the numerically obtained N_{xy}. This mismatch is owing to the fact that the mathematical form of non-Bloch transformation that we consider in the hopping terms while computing N_{xy}, employing PBC, is computed by employing a low-energy version of $H_\gamma(\mathbf{k})$. To obtain the low-energy spectrum of $H_\gamma(\mathbf{k})$, we expand the Hamiltonian around $\mathbf{k} = (0, 0)$. By doing that we can obtain the phase boundary associated with the right part of Fig. 5(b). However, when we incorporate the higher-order hopping elements, the low-energy model around $\mathbf{k} = (0, 0)$ does not necessarily encapsulate all the phase transition lines. In that scenarion, one should also consider a low-energy Hamiltonian around other momenta such as $\mathbf{k} = (\pm 2\pi/3, \pm 2\pi/3)$, depending upon the value of m_0. Nevertheless, this scenario adds substantial complexity to the problem as one should consider a different non-Bloch form for different m_0. Thus, finding a universal transformation to obtain the exact phase boundary in the NH second NN hopping case still remains an interesting question and beyond the scope of the present paper. Nevertheless, complex energy spectra under PBC might be useful for understanding the phase boundaries between two different topological phases.

IV. SUMMARY AND CONCLUSION

To summarize, in this article, we consider a long-range hopping model in the presence of non-Hermiticity to investigate the emergence of second-order topological phases. By exploring the real part of the complex energy spectrum for the first and second NN NH models under OBC, we find that the former model only hosts four zero-energy corner modes while the latter model can host four as well as sixteen zero-energy corner modes as the hallmark of the NH SOTI phases. We compute the real space invariant namely, bi-orthogonalized QWN, by keeping in mind the non-Bloch form of the momentum to uniquely characterize the different topological phases. The phase boundaries, captured by the above invariant, can successfully mimic the emergence of NH SOTI phases out of the trivial phases, as demonstrated by the complex energy dispersion under OBC for both the first and second NN models. The topological phase boundary between two different topological phases, observed in the second NN model, can be anticipated from the complex energy spectrum under PBC for the above model. In the future, one can include disorder to study the exceptional topological Anderson insulators hosting corner modes where a generalized version of the presently adopted real space topological index will have to be examined.

Acknowledgments

A.K.G. and A.S. acknowledge SAMKHYA: High-Performance Computing Facility provided by Institute of Physics, Bhubaneswar, for numerical computations. TN acknowledges the NFSG “NFSG/HYD/2023/H0911” from BITS Pilani.

[1] M. Z. Hasan and C. L. Kane, *“Colloquium: topological insulators,”* Rev. Mod. Phys. **82**, 3045 (2010).
[2] M. Sato and Y. Ando, *“Topological superconductors: a review,”* Reports on Progress in Physics **80**, 076501 (2017).
[3] F. D. M. Haldane, *“Model for a Quantum Hall Effect without Landau Levels: Condensed-Matter Realization of the“Parity Anomaly”,”* Phys. Rev. Lett. **61**, 2015 (1988).
[4] C. L. Kane and E. J. Mele, *“Z_2 Topological Order and the Quantum Spin Hall Effect,”* Phys. Rev. Lett. **95**, 146802 (2005).
[5] B. A. Bernevig, T. L. Hughes, and S.-C. Zhang, *“Quantum spin Hall effect and topological phase transition in HgTe quantum wells,”* Science **314**, 1757 (2006).
[6] W. A. Benalcazar, B. A. Bernevig, and T. L. Hughes, *“Quantized electric multipole insulators,”* Science **357**, 61 (2017).
[7] W. A. Benalcazar, B. A. Bernevig, and T. L. Hughes, *“Electric multipole moments, topological multipole moment pumping, and chiral hinge states in crystalline in-*

sulators," Phys. Rev. B **96**, 245115 (2017).

[8] Z. Song, Z. Fang, and C. Fang, *"$(d-2)$-Dimensional Edge States of Rotation Symmetry Protected Topological States,"* Phys. Rev. Lett. **119**, 246402 (2017).

[9] J. Langbehn, Y. Peng, L. Trifunovic, F. von Oppen, and P. W. Brouwer, *"Reflection-Symmetric Second-Order Topological Insulators and Superconductors,"* Phys. Rev. Lett. **119**, 246401 (2017).

[10] F. Schindler, A. M. Cook, M. G. Vergniory, Z. Wang, S. S. Parkin, B. A. Bernevig, and T. Neupert, *"Higher-order topological insulators,"* Science adv. **4**, eaat0346 (2018).

[11] S. Franca, J. van den Brink, and I. C. Fulga, *"An anomalous higher-order topological insulator,"* Phys. Rev. B **98**, 201114 (2018).

[12] Z. Wang, B. J. Wieder, J. Li, B. Yan, and B. A. Bernevig, *"Higher-Order Topology, Monopole Nodal Lines, and the Origin of Large Fermi Arcs in Transition Metal Dichalcogenides $X\mathrm{Te}_2$ ($X = \mathrm{Mo, W}$),"* Phys. Rev. Lett. **123**, 186401 (2019).

[13] D. Călugăru, V. Juričić, and B. Roy, *"Higher-order topological phases: A general principle of construction,"* Phys. Rev. B **99**, 041301 (2019).

[14] P. Szumniak, D. Loss, and J. Klinovaja, *"Hinge modes and surface states in second-order topological three-dimensional quantum Hall systems induced by charge density modulation,"* Phys. Rev. B **102**, 125126 (2020).

[15] X. Ni, M. Li, M. Weiner, A. Alù, and A. B. Khanikaev, *"Demonstration of a quantized acoustic octupole topological insulator,"* Nature Communications **11**, 2108 (2020).

[16] B. Xie, H. Wang, X. Zhang, P. Zhan, J. Jiang, M. Lu, and Y. Chen, *"Higher-order band topology,"* Nat. Rev. Phys. **3**, 520 (2021).

[17] S. Saha, T. Nag, and S. Mandal, "Dipolar quantum spin Hall insulator phase in extended Haldane model," (2022), arXiv:2204.06641.

[18] X. Zhu, *"Tunable Majorana corner states in a two-dimensional second-order topological superconductor induced by magnetic fields,"* Phys. Rev. B **97**, 205134 (2018).

[19] T. Liu, J. J. He, and F. Nori, *"Majorana corner states in a two-dimensional magnetic topological insulator on a high-temperature superconductor,"* Phys. Rev. B **98**, 245413 (2018).

[20] Z. Yan, F. Song, and Z. Wang, *"Majorana Corner Modes in a High-Temperature Platform,"* Phys. Rev. Lett. **121**, 096803 (2018).

[21] Y. Wang, M. Lin, and T. L. Hughes, *"Weak-pairing higher order topological superconductors,"* Phys. Rev. B **98**, 165144 (2018).

[22] R.-X. Zhang, W. S. Cole, and S. Das Sarma, *"Helical Hinge Majorana Modes in Iron-Based Superconductors,"* Phys. Rev. Lett. **122**, 187001 (2019).

[23] R.-X. Zhang, W. S. Cole, X. Wu, and S. Das Sarma, *"Higher-Order Topology and Nodal Topological Superconductivity in Fe(Se,Te) Heterostructures,"* Phys. Rev. Lett. **123**, 167001 (2019).

[24] Y. Volpez, D. Loss, and J. Klinovaja, *"Second-Order Topological Superconductivity in π-Junction Rashba Layers,"* Phys. Rev. Lett. **122**, 126402 (2019).

[25] Z. Yan, *"Majorana corner and hinge modes in second-order topological insulator/superconductor heterostructures,"* Phys. Rev. B **100**, 205406 (2019).

[26] S. A. A. Ghorashi, X. Hu, T. L. Hughes, and E. Rossi, *"Second-order Dirac superconductors and magnetic field induced Majorana hinge modes,"* Phys. Rev. B **100**, 020509 (2019).

[27] Y.-J. Wu, J. Hou, Y.-M. Li, X.-W. Luo, X. Shi, and C. Zhang, *"In-Plane Zeeman-Field-Induced Majorana Corner and Hinge Modes in an s-Wave Superconductor Heterostructure,"* Phys. Rev. Lett. **124**, 227001 (2020).

[28] K. Laubscher, D. Chughtai, D. Loss, and J. Klinovaja, *"Kramers pairs of Majorana corner states in a topological insulator bilayer,"* Phys. Rev. B **102**, 195401 (2020).

[29] B. Roy, *"Higher-order topological superconductors in $\mathcal{P}$-, $\mathcal{T}$-odd quadrupolar Dirac materials,"* Phys. Rev. B **101**, 220506 (2020).

[30] S.-B. Zhang, W. B. Rui, A. Calzona, S.-J. Choi, A. P. Schnyder, and B. Trauzettel, *"Topological and holonomic quantum computation based on second-order topological superconductors,"* Phys. Rev. Research **2**, 043025 (2020).

[31] M. Kheirkhah, Z. Yan, and F. Marsiglio, *"Vortex-line topology in iron-based superconductors with and without second-order topology,"* Phys. Rev. B **103**, L140502 (2021).

[32] Z. Yan, *"Higher-Order Topological Odd-Parity Superconductors,"* Phys. Rev. Lett. **123**, 177001 (2019).

[33] J. Ahn and B.-J. Yang, *"Higher-order topological superconductivity of spin-polarized fermions,"* Phys. Rev. Research **2**, 012060 (2020).

[34] X.-J. Luo, X.-H. Pan, and X. Liu, *"Higher-order topological superconductors based on weak topological insulators,"* Phys. Rev. B **104**, 104510 (2021).

[35] Q. Wang, C.-C. Liu, Y.-M. Lu, and F. Zhang, *"High-Temperature Majorana Corner States,"* Phys. Rev. Lett. **121**, 186801 (2018).

[36] A. K. Ghosh, T. Nag, and A. Saha, *"Hierarchy of higher-order topological superconductors in three dimensions,"* Phys. Rev. B **104**, 134508 (2021).

[37] B. Roy and V. Juričić, *"Mixed-parity octupolar pairing and corner Majorana modes in three dimensions,"* Phys. Rev. B **104**, L180503 (2021).

[38] T. Li, M. Geier, J. Ingham, and H. D. Scammell, *"Higher-order topological superconductivity from repulsive interactions in kagome and honeycomb systems,"* 2D Materials **9**, 015031 (2021).

[39] A. K. Ghosh, T. Nag, and A. Saha, *"Systematic generation of the cascade of anomalous dynamical first- and higher-order modes in Floquet topological insulators,"* Phys. Rev. B **105**, 115418 (2022).

[40] A. K. Ghosh, T. Nag, and A. Saha, *"Dynamical construction of quadrupolar and octupolar topological superconductors,"* Phys. Rev. B **105**, 155406 (2022).

[41] W. DeGottardi, M. Thakurathi, S. Vishveshwara, and D. Sen, *"Majorana fermions in superconducting wires: Effects of long-range hopping, broken time-reversal symmetry, and potential landscapes,"* Phys. Rev. B **88**, 165111 (2013).

[42] Y. Niu, S. B. Chung, C.-H. Hsu, I. Mandal, S. Raghu, and S. Chakravarty, *"Majorana zero modes in a quantum Ising chain with longer-ranged interactions,"* Phys. Rev. B **85**, 035110 (2012).

[43] D. Xie, W. Gou, T. Xiao, B. Gadway, and B. Yan, *"Topological characterizations of an extended Su–Schrieffer–Heeger model,"* npj Quantum Information **5**, 55 (2019).

[44] R. G. Dias and A. M. Marques, *"Long-range hopping and indexing assumption in one-dimensional topological insulators,"* Phys. Rev. B **105**, 035102 (2022).

[45] M. Thakurathi, A. A. Patel, D. Sen, and A. Dutta, *"Floquet generation of Majorana end modes and topological invariants,"* Phys. Rev. B **88**, 155133 (2013).

[46] A. P. Schnyder, S. Ryu, A. Furusaki, and A. W. W. Ludwig, *"Classification of topological insulators and superconductors in three spatial dimensions,"* Phys. Rev. B **78**, 195125 (2008).

[47] A. Kitaev, in *AIP conference proceedings*, Vol. 1134 (American Institute of Physics, 2009) pp. 22–30.

[48] S. Ryu, A. P. Schnyder, A. Furusaki, and A. W. Ludwig, *"Topological insulators and superconductors: tenfold way and dimensional hierarchy,"* New Journal of Physics **12**, 065010 (2010).

[49] S. Ryu and Y. Hatsugai, *"Topological Origin of Zero-Energy Edge States in Particle-Hole Symmetric Systems,"* Phys. Rev. Lett. **89**, 077002 (2002).

[50] J. C. Y. Teo and C. L. Kane, *"Topological defects and gapless modes in insulators and superconductors,"* Phys. Rev. B **82**, 115120 (2010).

[51] M. Nakahara, *Geometry, topology and physics* (CRC press, 2018).

[52] W. A. Benalcazar and A. Cerjan, *"Chiral-Symmetric Higher-Order Topological Phases of Matter,"* Phys. Rev. Lett. **128**, 127601 (2022).

[53] N. Parappurath, F. Alpeggiani, L. Kuipers, and E. Verhagen, *"Direct observation of topological edge states in silicon photonic crystals: Spin, dispersion, and chiral routing,"* Science Advances **6**, eaaw4137 (2020).

[54] Y. Yang, Z. Gao, H. Xue, L. Zhang, M. He, Z. Yang, R. Singh, Y. Chong, B. Zhang, and H. Chen, *"Realization of a three-dimensional photonic topological insulator,"* Nature **565**, 622 (2019).

[55] S. Malzard, C. Poli, and H. Schomerus, *"Topologically Protected Defect States in Open Photonic Systems with Non-Hermitian Charge-Conjugation and Parity-Time Symmetry,"* Phys. Rev. Lett. **115**, 200402 (2015).

[56] A. Regensburger, C. Bersch, M.-A. Miri, G. Onishchukov, D. N. Christodoulides, and U. Peschel, *"Parity–time synthetic photonic lattices,"* Nature **488**, 167 (2012).

[57] R. El-Ganainy, K. G. Makris, M. Khajavikhan, Z. H. Musslimani, S. Rotter, and D. N. Christodoulides, *"Non-Hermitian physics and PT symmetry,"* Nature Physics **14**, 11 (2018).

[58] M. M. Denner, A. Skurativska, F. Schindler, M. H. Fischer, R. Thomale, T. Bzdušek, and T. Neupert, *"Exceptional topological insulators,"* Nature Communications **12**, 5681 (2021).

[59] E. J. Bergholtz and J. C. Budich, *"Non-Hermitian Weyl physics in topological insulator ferromagnet junctions,"* Phys. Rev. Research **1**, 012003 (2019).

[60] Y.-B. Yang, K. Li, L.-M. Duan, and Y. Xu, *"Higher-order topological Anderson insulators,"* Phys. Rev. B **103**, 085408 (2021).

[61] P. San-Jose, J. Cayao, E. Prada, and R. Aguado, *"Majorana bound states from exceptional points in non-topological superconductors,"* Scientific Reports **6**, 21427 (2016).

[62] V. Kozii and L. Fu, "Non-Hermitian topological theory of finite-lifetime quasiparticles: prediction of bulk Fermi arc due to exceptional point," arXiv:1708.05841.

[63] T. Yoshida, R. Peters, and N. Kawakami, *"Non-Hermitian perspective of the band structure in heavy-fermion systems,"* Phys. Rev. B **98**, 035141 (2018).

[64] H. Shen and L. Fu, *"Quantum Oscillation from In-Gap States and a Non-Hermitian Landau Level Problem,"* Phys. Rev. Lett. **121**, 026403 (2018).

[65] Z. H. Musslimani, K. G. Makris, R. El-Ganainy, and D. N. Christodoulides, *"Optical Solitons in $\mathcal{PT}$ Periodic Potentials,"* Phys. Rev. Lett. **100**, 030402 (2008).

[66] K. G. Makris, R. El-Ganainy, D. N. Christodoulides, and Z. H. Musslimani, *"Beam Dynamics in $\mathcal{PT}$ Symmetric Optical Lattices,"* Phys. Rev. Lett. **100**, 103904 (2008).

[67] S. Yao, F. Song, and Z. Wang, *"Non-Hermitian Chern Bands,"* Phys. Rev. Lett. **121**, 136802 (2018).

[68] K. Kawabata, K. Shiozaki, M. Ueda, and M. Sato, *"Symmetry and Topology in Non-Hermitian Physics,"* Phys. Rev. X **9**, 041015 (2019).

[69] E. J. Bergholtz, J. C. Budich, and F. K. Kunst, *"Exceptional topology of non-Hermitian systems,"* Rev. Mod. Phys. **93**, 015005 (2021).

[70] K. Sone, Y. Ashida, and T. Sagawa, *"Exceptional non-Hermitian topological edge mode and its application to active matter,"* Nature Communications **11**, 5745 (2020).

[71] A. K. Ghosh and A. M. Black-Schaffer, "Majorana zero-modes in a dissipative Rashba nanowire," arXiv:2403.00419.

[72] S. Yao and Z. Wang, *"Edge States and Topological Invariants of Non-Hermitian Systems,"* Phys. Rev. Lett. **121**, 086803 (2018).

[73] F. K. Kunst, E. Edvardsson, J. C. Budich, and E. J. Bergholtz, *"Biorthogonal Bulk-Boundary Correspondence in Non-Hermitian Systems,"* Phys. Rev. Lett. **121**, 026808 (2018).

[74] T. Liu, Y.-R. Zhang, Q. Ai, Z. Gong, K. Kawabata, M. Ueda, and F. Nori, *"Second-Order Topological Phases in Non-Hermitian Systems,"* Phys. Rev. Lett. **122**, 076801 (2019).

[75] T. Helbig, T. Hofmann, S. Imhof, M. Abdelghany, T. Kiessling, L. W. Molenkamp, C. H. Lee, A. Szameit, M. Greiter, and R. Thomale, *"Generalized bulk–boundary correspondence in non-Hermitian topolectrical circuits,"* Nature Physics **16**, 747 (2020).

[76] D. S. Borgnia, A. J. Kruchkov, and R.-J. Slager, *"Non-Hermitian Boundary Modes and Topology,"* Phys. Rev. Lett. **124**, 056802 (2020).

[77] R. Koch and J. C. Budich, *"Bulk-boundary correspondence in non-Hermitian systems: stability analysis for generalized boundary conditions,"* The European Physical Journal D **74**, 70 (2020).

[78] H.-G. Zirnstein, G. Refael, and B. Rosenow, *"Bulk-Boundary Correspondence for Non-Hermitian Hamiltonians via Green Functions,"* Phys. Rev. Lett. **126**, 216407 (2021).

[79] Y. Takane, *"Bulk–Boundary Correspondence in a Non-Hermitian Chern Insulator,"* Journal of the Physical Society of Japan **90**, 033704 (2021).

[80] K. Kawabata, M. Sato, and K. Shiozaki, *"Higher-order non-Hermitian skin effect,"* Phys. Rev. B **102**, 205118 (2020).

[81] C. M. Bender, *"Making sense of non-Hermitian Hamiltonians,"* Rep. Prog. Phys. **70**, 947 (2007).

[82] W. D. Heiss, *"The physics of exceptional points,"* J. Phys. A: Math. Theor. **45**, 444016 (2012).

[83] B. Pérez-González, M. Bello, A. Gómez-León, and G. Platero, *"Interplay between long-range hopping and disorder in topological systems,"* Phys. Rev. B **99**, 035146 (2019).

[84] F. A. An, E. J. Meier, and B. Gadway, *"Engineering a Flux-Dependent Mobility Edge in Disordered Zigzag Chains,"* Phys. Rev. X **8**, 031045 (2018).

[85] H.-C. Hsu and T.-W. Chen, *"Topological Anderson insulating phases in the long-range Su-Schrieffer-Heeger model,"* Phys. Rev. B **102**, 205425 (2020).

[86] A. K. Ghosh and T. Nag, *"Non-Hermitian higher-order topological superconductors in two dimensions: Statics and dynamics,"* Phys. Rev. B **106**, L140303 (2022).

[87] H. Liu, J.-K. Zhou, B.-L. Wu, Z.-Q. Zhang, and H. Jiang, *"Real-space topological invariant and higher-order topological Anderson insulator in two-dimensional non-Hermitian systems,"* Phys. Rev. B **103**, 224203 (2021).

[88] H. Liu, M. Lu, Z.-Q. Zhang, and H. Jiang, *"Modified generalized Brillouin zone theory with on-site disorder,"* Phys. Rev. B **107**, 144204 (2023).

[89] D. Mondal and T. Nag, "Persistent anomaly in dynamical quantum phase transition in long-range non-Hermitian p-wave Kitaev chian," arXiv:2402.04603.

[90] C.-K. Chiu, J. C. Y. Teo, A. P. Schnyder, and S. Ryu, *"Classification of topological quantum matter with symmetries,"* Rev. Mod. Phys. **88**, 035005 (2016).

[91] L. Lin, Y. Ke, and C. Lee, *"Real-space representation of the winding number for a one-dimensional chiral-symmetric topological insulator,"* Phys. Rev. B **103**, 224208 (2021).